IMPROVED EVALUATION OF (HYPER-)CEST IMAGES USING THE SPECTRAL DIMENSION

Jörg Döpfert[1], Christopher Witte[1], Martin Kunth[1], Michael Beyermann[1], and Leif Schröder[1]
[1]*Leibniz-Institut für Molekulare Pharmakologie (FMP), Berlin, Germany*

Introduction:

Hyperpolarized xenon can be used as a contrast agent in solution due to its solubility in water. Its excellent chemical shift sensitivity motivated the design of xenon biosensors [1]. Even though the detection of quite low concentrations of such sensors has been demonstrated by the Hyper-CEST technique [2, 3], the detected Xe solution peak often suffers from low signal intensity. Here, we address the problem of detecting systematic signal changes in this peak due to the Chemical Exchange Saturation Transfer (CEST) effect. A selective saturation pulse is used to deplete the polarization of atoms bound to the biosensor. Through chemical exchange, this signal is transferred to the solution peak. The normalized CEST effect per pixel $C(x,y)$ is typically determined by subtracting an image acquired with the saturation pulse irradiating on resonant with Xe in the biosensor (S_{on}) from an off resonant image (S_{off}): $C = (S_{off} - S_{on}) / S_{off}$ [4] . In this work, we present two alternative approaches, based on least squares fitting (LSF) and principal component analysis (PCA), that treat an entire sequence of CEST images, with a range of different saturation frequencies, as a single spectral image. We apply both approaches to low signal to noise ratio (SNR) Hyper-CEST xenon images of a sample with two CEST peaks that are separated by ~1 ppm and compare the results to standard off and on resonant saturation. The proposed methods may also be readily applied to conventional proton CEST imaging.

Methods:

The imaged phantom (Fig. 1) consisted of an inner (IC) and an outer compartment (OC). The IC contained a solution of agent 1 (cryptophane-A monoacid (CrA), 50µM) and the OC contained a solution of agent 2 (CrA attached to NH-PEG$_2$-COOH, 50µM), yielding exchanging resonances at ω_1 = 59 ppm and ω_2 = 60 ppm with respect to the xenon gas peak, respectively. Xe was bubbled into solution as described elsewhere [5]. 21 CEST images where acquired on a 9.4 T NMR spectrometer after CW saturation (t = 3s, B_1 = 0.6µT, ω_{sat} = [58.7 - 60.5] ppm) with an EPI readout (matrix 32x32, FOV (2cm)^2). Two methods were employed to evaluate the image stack:

I) LSF: We fit the pixel intensities of the CEST images to a double lorentzian curve [6], $S(\omega) = A_0 - \frac{I_1}{1+((\omega-\omega_1)/\gamma_1)^2} - \frac{I_2}{1+((\omega-\omega_2)/\gamma_2)^2}$,

where ω is the frequency of the saturation pulse, A_0 is the baseline offset, and ω_1 and ω_2 are the resonant frequencies of agents 1 and 2 respectively with widths of γ_1 and γ_2 and intensities I_1 and I_2. Initial fit parameters were estimated by fitting the above equation to the mean image intensities $I_{Av}(\omega)$, averaged over all 32x32 pixels for each saturation frequency ω. We then fit individual pixel intensities $I(x,y,\omega)$ to the same equation but only varying the offset A_0 and the intensity of the two lorentzians, I_1 and I_2. The resulting parameter maps $I_1(x,y)$ and $I_2(x,y)$ were used to represent the signal of the two agents.

II) PCA: Looking at the image stack as a series of z-spectra, one for each pixel, it is easy to see it is highly redundant. Many pixels vary (as a function of saturation frequency) in a similar fashion, for instance the pixels in the inner compartment all decrease in intensity as the saturation approaches 59 ppm. PCA [7] exploits this redundancy to deconstruct the data set into a series of principal components or "eigenspectra" and ranks them according to how much of the data's variance they describe. By reproducing the data set with just the highest ranked principal components we can remove much of the noise in the data set. We discovered that using only the two highest ranked principal components was sufficient to reliably reproduce the entire image stack and eliminate much of the noise. Using this reconstructed data set we then calculated the signal $C(x,y)$ of the two agents using the standard CEST subtraction.

Results and discussion:

The proton image in Fig. 1 depicts the two compartments of the phantom as well as the capillaries used to bubble hyperpolarized xenon into solution. Though the xenon CEST images shown in Fig. 2 are noisy, it can clearly be seen that by saturating at different frequencies we can selectively destroy the signal from either the inner or the outer compartment to localize the different agents, even though their resonances are only separated by 1 ppm. Fig. 3a) shows a false colour image where signal from the agents is calculated in the conventional manner by subtracting either of the two on resonant images at ω_1 = 59 ppm (agent 1, depicted in green) or at ω_2 = 60 ppm (agent 2, depicted in red) from an off resonant image. To ensure comparability, the 3 datasets were averaged 7 times each, yielding 21 images in total. In Fig. 2b) and c) we see the results where the signal from the different agents was determined by LSF and PCA respectively. By utilising the information from a range of saturation frequencies, both methods significantly improve the localization of the agents and increase the SNR by a factor of 1.6 and 1.4 for LSF and PCA respectively (IC) and by a factor of 1.7 and 1.8 for LSF and PCA respectively (OC). Moreover, in contrast to the standard subtraction, prior knowledge of the exact resonance frequencies is not required for the proposed methods but comes along as an extra result. Additionally, further information about the exchanging agents can be extracted from the fit parameters obtained with LSF.

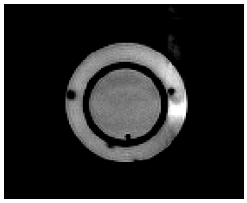

Fig. 1: T_2-weighted axial slice of the phantom showing the IC and the OC

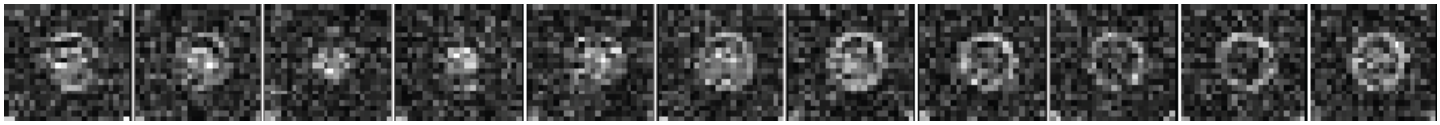

Fig. 2: Selected xenon Hyper-CEST images from the full series of 21 images, sweeping the saturation frequency between 58.7 and 60.5 ppm.

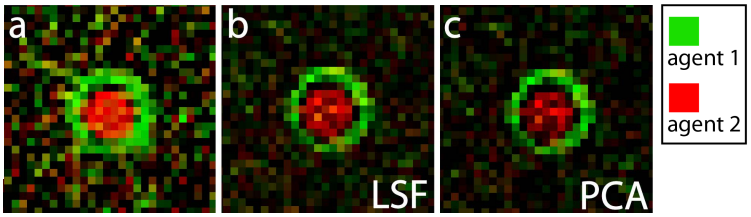

Fig. 3: False colour images with agent 1 in green and agent 2 in red, generated using a) standard CEST subtraction, b) the LSF approach and c) the PCA approach.

References

[1] Spence et al., PNAS, **98**, 10654 (2001)
[2] Schröder et al., Science, **314**, 446 (2006)
[3] Schröder et al., Phys. Rev. Lett., 100, 257603 (2008)
[4] Terreno et al., Contrast Media Mol. Imaging, **4**, 237 (2009)
[5] Han et al., Anal. Chem., **77**, 4008 (2005)
[6] Zaiss et al., J. Magn. Reson., **211**, 149 (2011)
[7] Jolliffe, *Principal Component Analysis*, Springer, New York (2002)